ISSN 1674-1056
http://cpb.iphy.ac.cn
http://iopscience.iop.org/cpb
中国物理 B
Chinese Physics
中国物理
Chinese Physics B

Effects of heat loss and viscosity friction at walls on flame acceleration and deflagration to detonation transition

Jin Huang(黄金), Wenhu Han(韩文虎), Xiangyu Gao(高向宇), Cheng Wang(王成)

Citation: Chin. Phys. B . 2019, 28(7): 074704. **doi:** 10.1088/1674-1056/28/7/074704
Journal homepage: http://cpb.iphy.ac.cn; http://iopscience.iop.org/cpb

What follows is a list of articles you may be interested in

Acoustic characteristics of pulse detonation engine with ellipsoidal reflector

Yang Kang(康杨), Ning Li(李宁), Chun-Sheng Weng(翁春生), Chuan-Wei Wang(王传位)
Chin. Phys. B . 2018, 27(10): 104703. **doi:** 10.1088/1674-1056/27/10/104703

Theoretical analysis on deflagration-to-detonation transition

Yun-Feng Liu(刘云峰), Huan Shen(沈欢), De-Liang Zhang(张德良), Zong-Lin Jiang(姜宗林)
Chin. Phys. B . 2018, 27(8): 084703. **doi:** 10.1088/1674-1056/27/8/084703

Combustion of a single magnesium particle in water vapor

Huang Li-Ya, Xia Zhi-Xun, Zhang Wei-Hua, Huang Xu, Hu Jian-Xin
Chin. Phys. B . 2015, 24(9): 094702. **doi:** 10.1088/1674-1056/24/9/094702

Flow characterization and dilution effects of N_2 and CO_2 on premixed CH_4/air flames in a swirl-stabilized combustor

Han Yue, Cai Guo-Biao, Wang Hai-Xing, Renou Bruno, Boukhalfa Abdelkrim
Chin. Phys. B . 2014, 23(3): 034704. **doi:** 10.1088/1674-1056/23/3/034704

Numerical and experimental study on shear coaxial injectors with hot hydrogen-rich gas/oxygen-rich gas and GH_2/GO_2

Jin Ping, Li Mao, Cai Guo-Biao
Chin. Phys. B . 2013, 22(4): 044701. **doi:** 10.1088/1674-1056/22/4/044701

Effects of heat loss and viscosity friction at walls on flame acceleration and deflagration to detonation transition*

Jin Huang(黄金)[1], Wenhu Han(韩文虎)[2,†], Xiangyu Gao(高向宇)[1], and Cheng Wang(王成)[2]

[1] *Beijing Priority Laboratory of Earthquake Engineering and Structural Retrofit, Beijing University of Technology, Beijing* 100124, *China*
[2] *State Key Laboratory of Explosion Science and Technology, Beijing Institute of Technology, Beijing* 100081, *China*

(Received 29 March 2019; revised manuscript received 26 April 2019; published online 11 June 2019)

The coupled effect of wall heat loss and viscosity friction on flame propagation and deflagration to detonation transition (DDT) in micro-scale channel is investigated by high-resolution numerical simulations. The results show that when the heat loss at walls is considered, the oscillating flame presents a reciprocating motion of the flame front. The channel width and Boit number are varied to understand the effect of heat loss on the oscillating flame and DDT. It is found that the oscillating propagation is determined by the competition between wall heat loss and viscous friction. The flame retreat is led by the adverse pressure gradient caused by thermal contraction, while it is inhibited by the viscous effects of wall friction and flame boundary layer. The adverse pressure gradient formed in front of a flame, caused by the heat loss and thermal contraction, is the main reason for the flame retreat. Furthermore, the oscillating flame can develop to a detonation due to the pressure rise by thermal expansion and wall friction. The transition to detonation depends non-monotonically on the channel width.

Keywords: micro-scale channel, heat loss, oscillating flame, deflagration to detonation transition (DDT)

PACS: 47.70.Pq, 47.40.Rs, 82.33.Vx **DOI:** 10.1088/1674-1056/28/7/074704

1. Introduction

Flame propagation and deflagration to detonation transition (DDT) depends strongly on tube diameter/channel width, so the role of wall conditions is extremely important.[1–3] In a relatively macro-scale channel ($\sim$ 10 mm or greater), turbulent flame acceleration and reactivity gradient mechanism are found to be the main reasons for DDT.[4,5] Previous studies have indicated that the channel width had effect on flame propagation, the run-up distance, and the mechanism of DDT.[6–9] However, heat transfer and viscous friction at the walls are important for flame acceleration and DDT in micro-scale channels ($\sim$ 0.1 mm).[10,11] Akkerman *et al.*[12] found that flame has a oscillating propagation speed due to variations of the curved flame shape. The wall friction due to viscosity was critical for the DDT in thin channels and substantiated the theoretical advances revealing the important role of hydraulic resistance in DDT[13,14] and detonation velocity deficit.[15–18] However, heat loss at walls was usually neglected by assuming no heat transfer at the pipe surface. In fact, both friction and heat loss at walls are critical for flame propagation and DDT in the micro-channel.[19–22] Recently, Wu *et al.*[23] experimentally studied ethylene-oxygen DDT in capillary channel, and observed oscillating flame at low equivalence ratio.

Recognizing the above worthwhile studies, we note that in a micro-scale channel, the effects of convective heat transfer at the wall and its coupling with the viscous friction on the oscillating flames have not been examined. It is not clear whether an oscillating flame can develop into detonation. The goal of this paper is to conduct high fidelity simulations of oscillating flames and the transition to detonation in micro-scale channels by considering the combined effect of wall heat loss and viscous friction.

2. Governing equations

The conservation equations including the compressible Navier–Stokes (NS) equations, with advection, diffusion, and reaction sources, are given by

$$\frac{\partial(\rho)}{\partial t}+\frac{\partial(\rho u_i)}{\partial x_i}=0, \tag{1}$$

$$\frac{\partial(\rho u_i)}{\partial t}+\frac{\partial}{\partial x_j}(\rho u_i u_j+\delta_{ij}p-\zeta_{ij})=0, \tag{2}$$

$$\frac{\partial}{\partial t}\left(\rho e+\frac{1}{2}\rho u_i u_i\right)+\frac{\partial}{\partial x_j}\left(\rho u_j h+\frac{1}{2}\rho u_i u_i u_j+\sigma_j-u_i\zeta_{ij}\right)=0, \tag{3}$$

$$\frac{\partial(\rho Y)}{\partial t}+\frac{\partial}{\partial x_j}\left(\rho u_i Y-\frac{\mu}{Sc}\frac{\partial Y}{\partial x_i}\right)=-A\rho^2 Y\exp(-E_a/R_pT), \tag{4}$$

$$p=\rho R_pT/M. \tag{5}$$

Here, ρ, p, u, and T are the density, pressure, velocity, and temperature, respectively; Y is the mass fraction, $e=QY+C_VT=QY+R_pT/(\gamma-1)$ is the internal energy, and

*Project supported by the National Natural Science Foundation of China (Grant Nos. 11732003 and 11521062) and the National Key Research and Development Program of China (Grant No. 2017YFC0804700).

†Corresponding author. E-mail: hanwenhu@bit.edu.cn

© 2019 Chinese Physical Society and IOP Publishing Ltd

$h = QY + C_pT = QY + R_pT\gamma/(\gamma-1)$ is the enthalpy, all of which are functions of space x and time t. Furthermore, Q is the heat of reaction, C_V and C_p are the specific heats at constant volume and constant pressure, respectively, R_p is the ideal gas constant, M is the molar mass, γ is the adiabatic exponent, and E_a and A are the activation energy and pre-exponential factor of the assumed one-step overall reaction, respectively. The stress tensor ζ_{ij} and the energy diffusion vector σ_j are respectively given by

$$\zeta_{ij} = \mu\left(\frac{\partial u_i}{\partial x_j} + \frac{\partial u_j}{\partial x_i} - \frac{2}{3}\frac{\partial u_k}{\partial x_k}\delta_{ij}\right), \tag{6}$$

$$\sigma_j = \mu\left(\frac{C_p}{Pr}\frac{\partial T}{\partial x_j} - \frac{Q}{Sc}\frac{\partial Y}{\partial x_j}\right). \tag{7}$$

Here, $\mu \equiv \rho\nu$ is the viscosity coefficient, ν is the kinematic viscosity, $Pr = 0.75$ and $Sc = 0.75$ are the Prandtl and Schmidt numbers, respectively, and δ_{ij} is the Kronecker delta. The flame thickness is defined as $f_l = \nu/PrS_l$, where S_l is laminar flame speed. The Reynolds number is defined as $Re = S_l d/\nu$, where d is the channel width.

A wave of premixed gas combustion spreading from the closed and open-ended channel is studied by direct numerical simulation of the two-dimensional Navier–Stokes equations for a compressible reactive flow. The energy release rate is modeled by one-step Arrhenius kinetics, which is assumed to be of the first order with respect to the deficient reactant and of the second order with respect to the density. This reaction rate is very fast so that rapid heat release is easy to produce a transition from a flame to a detonation.

To numerically solve the governing equations, we apply fifth order local characteristics based on the weighted essentially non-oscillatory (WENO) conservative finite difference scheme[24] to discretize the advection term and the sixth order central difference to the diffusion term, with third order total variation diminishing (TVD) Runge–Kutta time discretization.

3. Physical model and specifications

The computational domain is a two-dimensional (2D) channel. The channel width W is $2f_l$, $4f_l$, $8f_l$, and $16f_l$, respectively, while the channel length is 1200 f_l. A planar flame initiated by a weak ignition source is set at the left, with an expansion ratio of 10. In the unreacted mixture, the initial velocity, temperature, and pressure are 0.0 m/s, 300 K, and 1 atm, respectively. The physical model is shown in Fig. 1 and the mixture parameters are given in Table 1. The left is closed, while the right end is non-reflection boundary condition. Both the upper and lower boundaries are described by non-slip walls with adiabatic and heat-loss boundary conditions. The thermal loss at the left and right ends is neglected because the channel is very narrow. For adiabatic wall, there is $\partial T/\partial y = 0$; while $\partial T/\partial y = -Bi(T - T_0)$ for heat conducting walls, where Bi is Biot number denoting heat loss. In the following simulations, Bi is respectively 0, 7.5, and 10, which were used by Kagan *et al.*[4,19]

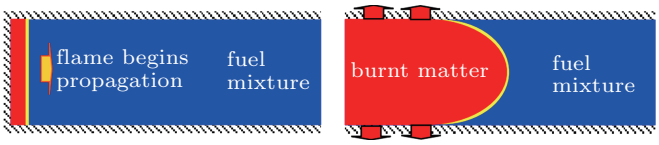


Fig. 1. Physical model.

Table 1. Thermo–physical properties of the gaseous mixture.[4,19]

γ	Q/J·Kg^{-1}	E_a	p_0/Pa	T_0/K	μ_0/m^2·s^{-1}	Le	Pr	f_l/m	S_l/m·s^{-1}
1.3	$18R_uT_0/M$	$20R_uT_0$	10^5	300	2.6×10^{-4}	1	0.75	6.5×10^{-5}	4.8

4. Results and discussions

4.1. Flame propagation with heat loss at walls

To verify grid convergence of the viscous detonation, we use the grid resolutions of 20 pts/f_l, 40 pts/f_l, and 60 pts/f_l to solve the NS solution for the case with $W = 8f_l$ and $Bi = 7.5$. Figure 2 shows that for the lower grid resolution, the solution differs obviously from those with higher resolution. However, the flame propagation with 40 pts/f_l is consistent with those of 60 pts/f_l, indicating that 40 pts/f_l is able to describe the entire process of DDT.

The temperature and pressure profiles along the wall are extracted at $tS_l/f_l = 189.5$, as shown in Fig. 2(b). It is seen that as the pressure wave becomes strong and the gradient forms, there are sufficient grid points to capture the temperature and pressure gradients. Hence, the present grid resolution is valid for DDT. The grid resolution of 40 pts/f_l is used for the following simulations. In the previous work of Wang *et al.*[25] and Han *et al.*,[17] the verification of grid resolution was done and demonstrated that good grid convergence can be obtained.

It is seen that in the process of flame propagation, oscillating motion occurs during $tS_l/f_l \sim 125$–200, resembling the observation in Ref. [21]. The oscillating flame eventually develops to a detonation at $tS_l/f_l \sim 207.5$. In the simulation, the open end is set as a non-reflection boundary condition so that the disturbance is not reflected from the end. Consequently, it is known that the backward motion of the flame front should be caused by the contraction resulting from the heat loss at walls. As the flame initially advances, the amount of heat loss at walls increases due to the longer high-temperature region at the walls. The flame decelerates and induces an expansion wave ahead of it, leading to an adverse pressure gradient in the upstream field. As a result, the reverse flow

in the upstream is observed, as shown in Fig. 3(a). Subsequently, during $tS_l/f_l \sim 40$–125, the reverse flow caused by the thermal contraction makes the fuel in the vicinity of the flame front flow inversely into the combustion front; the heat release balances the heat loss so that the flame propagates steadily. At $tS_l/f_l \sim 125$–200, the front elongates and the combustion temperature is higher; therefore, the accumulated heat loss renders it to decelerate and then retreat; the retreated flame is shortened and the combustion temperature decreases, which reduces the amount of heat loss at the wall. The thermal contraction is weakened, and the flame advances again due to the viscosity friction at the wall. Due to viscosity friction at walls, the flame surface near walls is extended so that the flame head appears near the walls, leading to the increase of the flame surface. Consequently, the increase of the flame area can enhance the heat release and makes the flame advance. Another role of viscosity friction is to enhance the temperature in the gas near walls and to shorten the ignition delay time. This enhances the burning rate of the gas near walls, which makes the formed flame head near walls go forward fast. Consequently, the oscillating flame forms, owing to the coupled role of thermal contraction and viscosity friction. The flame structure resembles globally the characteristics obtained by Akkerman *et al.*[12] and the unreacted gas in the gaps between the front surface and sidewalls is injected into the flame as it burns and the part that turns upstream can make the hump thrust, as shown in Fig. 3(b). The oscillating motion produces a complicated flow in the vicinity of the front, as shown in Fig. 3. The circulation flow in the flame is produced by the interaction of the positive-direction flow in the downstream with the reverse flow in the upstream, as shown in Fig. 3(e). This whirl flow significantly enhances the combustion rate of the preheated gas near the boundary layers, and the front near the boundary layer hence accelerates rapidly and develops toward the internal domain; the flame surface extends substantially. Simultaneously, the upstream flow near the boundary layers becomes positive-direction. The flame extends and moves forward, as shown in Fig. 3(f).

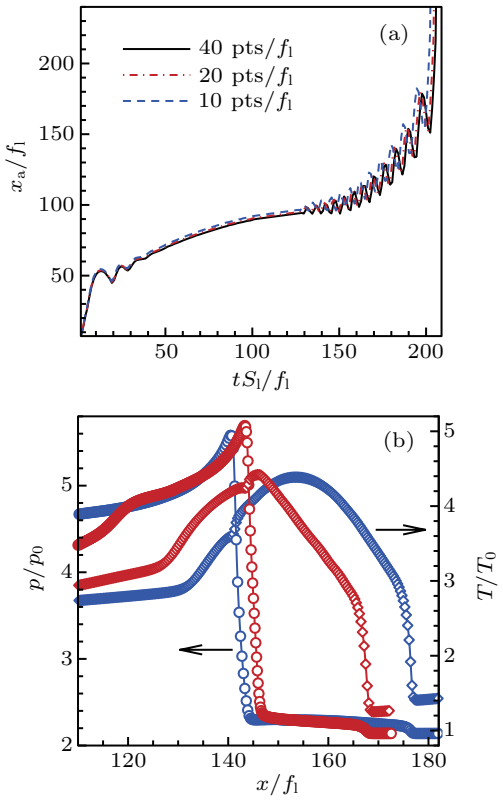


Fig. 2. Convergence of relative grid resolution for $W = 8f_l$ and $Bi = 7.5$; x_a denotes the flame-tip position that is defined as the flame surface at the center of the channel. (a) Flame tip vs. time for different grid resolutions; (b) the number of points in the pressure gradient at $tS_l/f_l = 189.5$.

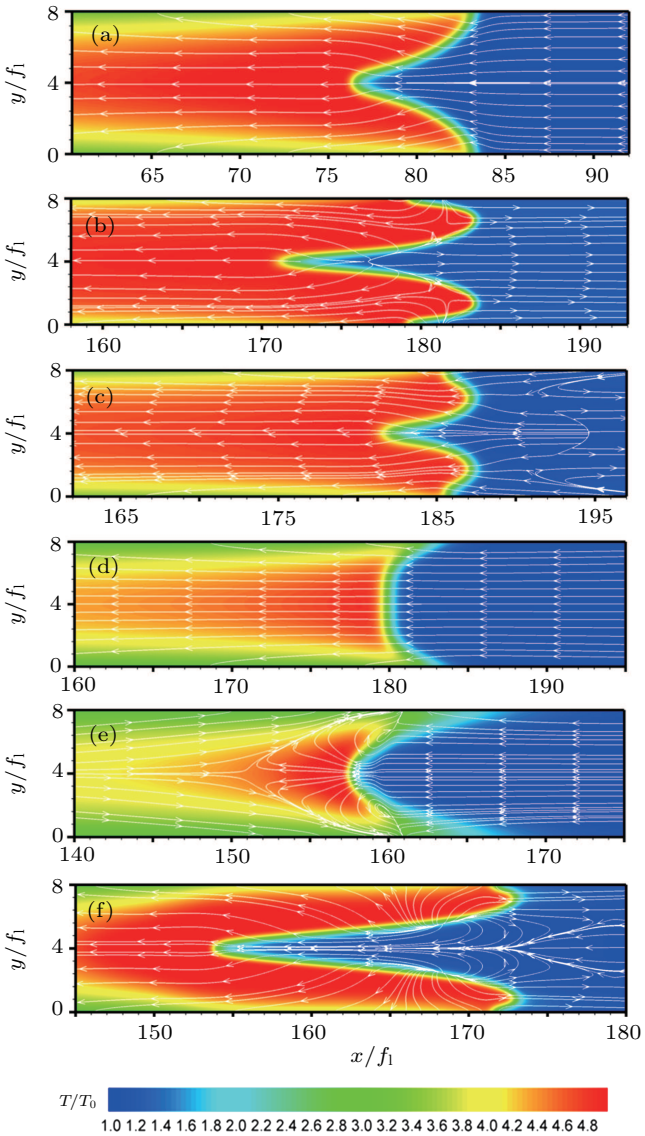


Fig. 3. Temperature contours in different stages: $tS_l/f_l =$ (a) 59.7, (b) 195.4, (c) 196.5, (d) 197.6, (e) 200.0, and (f) 201.2.

4.2. Effects of channel width and *Bi* number on flame propagation

Figure 4 shows the flame-tip position and flame speed as a function of time for different channel widths and *Bi* numbers. As $W = 8f_l$ is fixed, the adiabatic flame for $Bi = 0$ acceler-

ates and transits directly to a detonation. For $Bi = 7.5$, the oscillating flame appears; at $tS_l/f_l \sim 200$, the velocity jumps abruptly to ~ 390 (overdriven) and then decays to ~ 300. This may imply that in some situations, a locally strong oscillation in flame propagation can trigger the transition to a detonation. For $Bi = 10$, however, the flame accelerates more slowly in the initial stage. It begins to retreat at $tS_l/f_l \sim 20$ and then retreats oscillatorily. Eventually, DDT does not occur, as shown in Fig. 4. Therefore, the increase of Bi number reduces the flame acceleration rate during the initial period and suppresses the transition to a detonation.

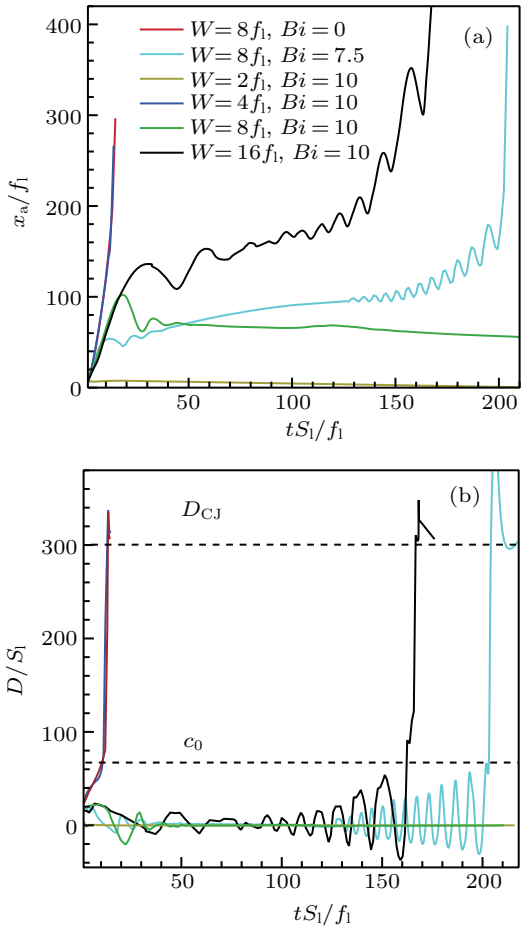


Fig. 4. Flame tip position as a function of time for different channel widths and Bi numbers. D, D_{CJ}, and c_0 are respectively flame speed, Chapman–Jouguet (CJ) velocity, and sonic speed in unreacted mixture. The lines in panel (b) correspond to the same color in panel (a).

At a fixed $Bi = 10$, an increase of the channel width changes flame propagation and the occurrence of DDT. For $W = 2f_l$, heat loss arrests the flame propagation, causing it to quench eventually. The unreacted gas ahead of the flame flows backward into the front due to the adverse pressure gradient. The effective heat release is not enough to sustain the flame and eventually the flame quenches, as shown in Fig. 5(a). For $W = 4f_l$, the reverse flow behind the front forms due to the wall heat loss. Approximately 50% of the product goes backward, and, for this reason, the flame acceleration rate is lower than that of the case without heat loss. Due to considerable elongation, the flame can still accelerate and develop to detonation. This indicates that the role of viscosity friction in flame elongation and flame acceleration is dominant in this case. For $W = 8f_l$, the stagnation plane behind the flame front shifts to the flame tip because the flame elongation is not enough to compensate for the negative effect led by heat loss, although the viscosity effect makes the flame elongated by the same length as that in the channel of $W = 4f_l$. As a result, the front starts to retreat at $x_a/f_l \sim 125$ and almost stops after several oscillations. Eventually, DDT does not occur. For $W = 16f_l$, the occurrence of oscillating flame is delayed, as compared with $W = 8f_l$. The flame begins to retreat at $x_a/f_l \sim 160$ and then propagates oscillatorily. Eventually, DDT occurs after a strong oscillation. In the wider channel, the role of heat loss and viscosity at walls in the flame acceleration is diminished. However, the flame can still accelerate due to hydrodynamic instability, although the stagnation plane shifts further to the flame tip, as shown in Fig. 5(d). Note that for $Bi = 10$, the wider channel of $W = 16f_l$ has earlier occurrence of DDT, compared to $W = 8f_l$ and $Bi = 7.5$. This is reasonable because for the wider channel, the heat-loss effect is weaker, while the hydrodynamic instability and viscosity is more important.

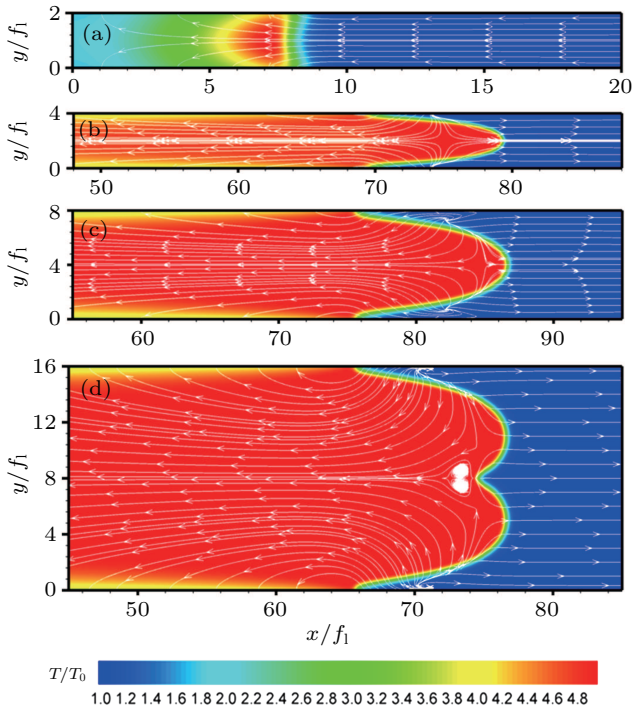


Fig. 5. Temperature contours and streamline in the stage of acceleration for $Bi = 10$: (a) $2f_l$, (b) $4f_l$, (c) $8f_l$, and (d) $16f_l$.

In summary, previous studies[12,26,27] indicated that during the flame acceleration phase, the whole new volume of the gas was pushed forward in the direction of the flame propagation. However, in the present simulation, a part of the product gas has reverse flow due to the heat loss at walls, which depends on the channel width.

4.3. Formation of oscillating flame and DDT

In this section, we choose the case of $W = 16f_l$ and $Bi = 10$ to reveal in more details the formation of the oscillating flame and DDT by inspecting the evolution of frontal structures and flow field. In the initial stage of oscillations, the flame shape and streamlines in the vicinity of the front are shown in Fig. 6. It is seen that at $tS_l/f_l = 27.6$, the flame surface is convex and more burnt gas behind the front goes backward due to thermal contraction. Consequently, the flame decelerates and induces an expansion wave ahead of it. As a result, the reverse flow in the upstream mixture forms due to the interaction of the expansion wave, which further makes the flame slow down and retreat; see Figs. 6(c), 6(d), and 6(e). As the flame goes back constantly, the amount of effective heat release decreases. At $tS_l/f_l = 45.6$, the front goes back to $x \sim 120$, and subsequently, the front near the boundary layers stops and the reaction rate is strengthened due to the wall friction. At $tS_l/f_l = 50.3$, the front near the boundary layer thrusts forward, with a large cusp; see Figs. 6(f) and 6(g). Consequently, the flame surface extends substantially and the effective heat release increases considerably at $tS_l/f_l = 49.7$. As the flame advances, the gap forms between the flame front and sidewalls at $tS_l/f_l = 52.9$; see Fig. 6(h). The gas in the gap is preheated due to viscosity friction, thereby enhancing the reaction rate. This effect makes the front near the wall further accelerate. At $tS_l/f_l = 55.5$–56.8, the flame accelerates globally and induces the pressure wave. While the unburned gas confined in the primary tulip cusp flows backward, the cusp moves forward, as shown in Figs. 6(i) and 6(j). The flame surface area decreases such that the released heat is not sufficient to meet the accumulated heat loss. The flame retreats again. Akkerman *et al.*[12] indicated that coupled role of thermal reaction and flow at the cusp caused oscillation of the flame speed, while it did not lead to reciprocation of the front motion. In their simulation, the heat transfer at walls was not considered, and the oscillating flame speed is caused by a "competition" between inertial force leading to the flame oscillations and the viscous force resulting in the flame acceleration. The study indicated that the inertial effects are important in the initial stage, while the viscous force dominates for self-similar flame acceleration at later stages. However, as the heat transfer is introduced, the oscillating flame results from the competition between the thermal contraction caused by heat loss and acceleration from viscosity friction. The burnt gas first expands at the flame front, but then the gas volume contracts because of the thermal loss to the walls. The volume contraction produces a flux in the direction of the burnt matter. In summary, in the initial stage, the flame retreat is mainly due to the accumulation of heat loss at walls as the flame elongates. The oscillating flame will be discussed later in more detail.

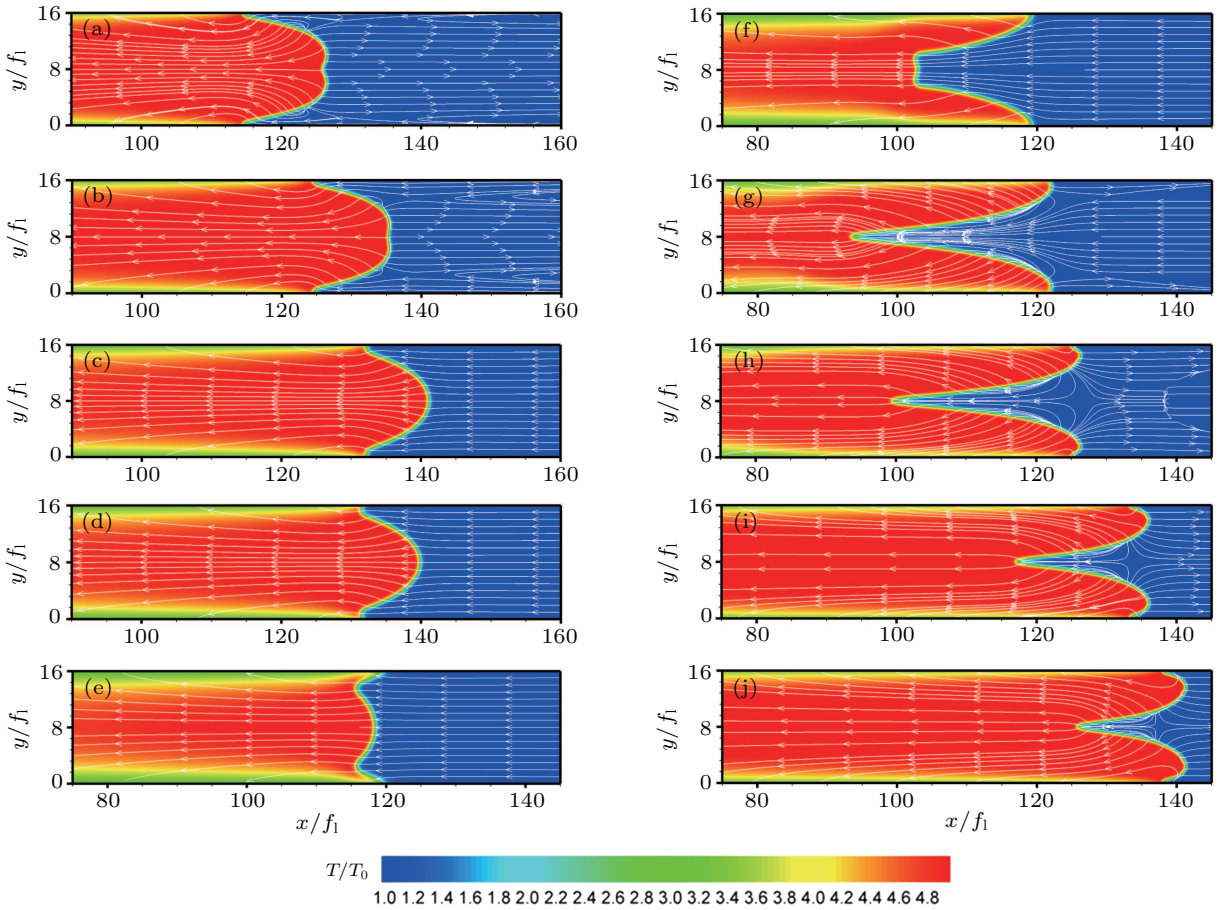


Fig. 6. Temperature contours and streamlines in the initial stage of oscillating flame: $tS_l/f_l =$ (a) 22.4, (b) 28.1, (c) 32.7, (d) 34.7, (e) 45.6, (f) 49.6, (g) 50.3, (h) 52.9, (i) 55.5, and (j) 56.8.

Figure 7 shows the pressure profiles at the centerline and wall in the vicinity of flame fronts shown in Fig. 6. We observe that at $tS_l/f_l = 22.4 - 32.7$ during which the flame retreats, the pressure decreases globally and the inverse pressure gradient presents due to heat loss. Note that at $tS_l/f_l = 55.5$, the oscillating flame accelerates rapidly and the positive pressure gradient steepens, indicating that a compression wave can form in front of the flame. The interaction of the compression wave produces a positive feedback mechanism for the transition to a detonation.

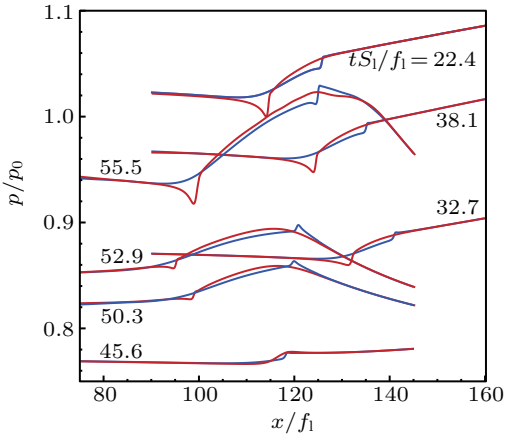


Fig. 7. Pressure distributions along the axis (red line) and the wall (blue line) near the flame fronts.

The flame shape and streamline are similar to that in the case of $W = 8f_l$ and $Bi = 7.5$, as shown in Fig. 8. From Fig. 8(a), the flame front globally starts to decelerate and the front near the boundary layer decelerates more significantly; see Figs. 8(a) and 8(b). Consequently, the front near wall first retreats, while the cusp in the middle still propagates forward, leading to the reduction of the flame surface. Consequently, the global front retreats at $tS_l/f_l = 114.5$ and 145.9; see Figs. 8(b) and 8(c). As the retreat decelerates and even stops, the circulation flow forms and leads to the burnt gas in the middle flame to the boundary. The flame near the boundary layer thrusts forward. The gas near the sidewall flows forward and turns to the middle, and then reflows into the tulip cusp due to the interaction of the reverse flow in the far upstream; see Fig. 8(d). As the flame accelerates globally, the positive-direction flow is amplified substantially so that it can offset the reverse flow far upstream at $tS_l/f_l = 149.1$; see Fig. 8(f). The gas confined in the tulip cusp still goes backward and further leads to the retreat of the cusp. As a result, the global flame extends substantially and the flame surface increases; see Fig. 8(g). Eventually, the flame can accelerate globally due to the large amount of heat released. For a wider channel, the frontal structure has more complicated evolution, compared with $W = 8f_l$ and $Bi = 7.5$. The elongation of the cusp is much larger during the oscillating stage, and hence the oscillating frequency is obviously lower, compared with $W = 8f_l$ and $Bi = 7.5$.

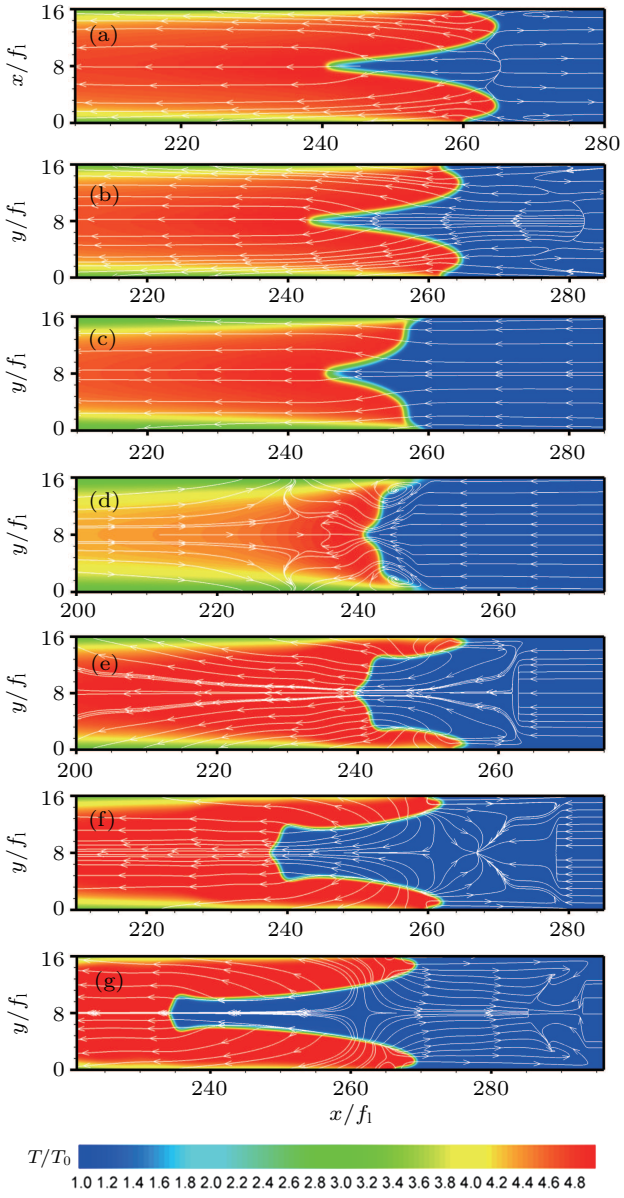


Fig. 8. Flame structure and streamlines in the oscillating flame: $tS_l/f_l =$ (a) 143.8, (b) 144.5, (c) 145.9, (d) 147.4, (e) 148.3, (f) 149.1, and (g) 150.0.

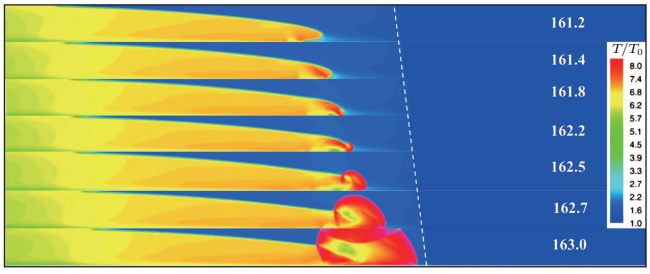


Fig. 9. Onset of detonation for $W = 16f_l$ and $Bi = 10$.

As the oscillations become stronger, the flame pulse induces a pressure wave that constantly compresses and preheats the gas mixture ahead it, reducing the induction time, as shown

in Fig. 9. As the strongly oscillating flame accelerates forward, local explosion in the gap between the flame surface and walls can be triggered due to wall friction, and eventually develops into detonation; see Fig. 9.

5. Conclusions

This work has numerically examined the flame propagation and DDT in a micro-scale channel with both viscous and heat loss effects at the walls. As the heat loss at the walls is introduced, the flame propagates oscillatorily, which is attributed to the competition between the flame elongation in a viscous boundary layer and the heat loss effects. It is found that the flame retreat is caused by the adverse pressure gradient due to the heat loss and thermal contraction. The net result of flame retreat and acceleration leads to an oscillating motion. The oscillating flame is likely to develop to a detonation due to the pressure rise by thermal compression and wall viscous friction. The occurrence of DDT depends non-monotonically on the channel width.

Kagan *et al.*[19] have used the reaction model of $n = 2$ to investigate the transition from a flame to a detonation in a channel. The studies[4,17,28] indicated that DDT is more likely to occur when the reaction level of $n = 2$ is considered, while it takes long time and distance for monomolecular reaction kinetics ($n = 1$). The present reaction model is valid for DDT because this study pays more attention to the physical mechanism, and the chemistry mechanism is relatively weak. Chen *et al.*[29] and Pan *et al.*[30,31] demonstrated that for super knocking in a combustion chamber, the detailed chemistry needs to be used to describe the autoignition and DDT. Furthermore, for some fuels with multi-stage ignition behavior and low-temperature chemistry, the real chemistry needs to be considered for DDT in a micro-channel. This merits study in future works.

For the effect of the ignition method, Kagan *et al.*[19] indicated that the planar ignition and point ignition causes a difference in the initial flame propagation, while the global trend is uniform for these two ignition methods. Under the point ignition, the flame initially assumes a nearly spherical shape, and the flame undergoes an acceleration noticeably stronger than in the case of planar ignition. The flame velocity reaches its local maximum when the flame touches the wall. Note the oscillatory character of the incipient dynamics under isothermic boundary conditions. The change from planar to point ignition results in the enhancement of the incipient acceleration of the flame and slight reduction of the predetonation time and distance.

References

[1] Lee J H S 2008 *The Detonation Phenomenon* (Cambridge: Cambridge University Press)
[2] Gamezo V N, Khokhlov A M and Oran E S 2001 *Combust. Flame* **126** 1810
[3] Wu M H, Burke M P, Son S F and Yetter R A 2007 *Proc. Combust. Inst.* **31** 2429
[4] Kagan L and Sivashinsky G 2003 *Combus. Flame* **134** 389
[5] Liberman M A, Kuznetsov M, Ivanov A and Matsukov I 2009 *Phys. Lett. A* **373** 501
[6] Kerampran S, Desbordes D, Veyssière B and Bauwens L 2001 *AIAA* **1082**
[7] Khokhlov A M, Oran E S and Thomas G O 1999 *Combust. Flame* **117** 323
[8] Brailovsky I, Kagan L and Sivashinsky G 2012 *Phil. Trans. R. Soc. A* **370** 625
[9] Tsuboi N, Morii Y and Hayashi A K 2013 *Proc. Combust. Inst.* **34** 1999
[10] Brailovsky I, Goldshtein V, Schreiber I and Sivashinsky G I 1997 *Combust. Sci. Tech.* **124** 145
[11] Valiev D, Bychkov V, Akkerman V, Eriksson L E and Marklund M 2008 *Phys. Lett. A* **372** 4850
[12] Akkerman V, Bychkov V, Petchenko A and Eriksson L E 2006 *Combust. Flame* **145** 675
[13] Liberman M A, Sivashinsky G I, Valiev D H and Eriksson L E 2006 *Int. J. Tran. Phenom.* **8** 253
[14] Brailovsky I and Sivashinsky G 2000 *Combust. Flame* **122** 492
[15] Brailovsky I and Sivashinsky G 1998 *Combust. Theor. Model.* **2** 429
[16] Kagan L and Sivashinsky G 2003 *Combust. Flame* **134** 389
[17] Han W H, Gao Y and Law C K 2017 *Combust. Flame* **176** 285
[18] Wang C, Zhao Y Y and Han W H 2017 *Combust. Sci. Technol.* **189** 1605
[19] Kagan L 2007 *Math. Model. Nat. Phenom.* **2** 40
[20] Ju Y and Law C K 2002 *Combust. Flame* **129** 356
[21] Ott J D, Oran E S and Anderson J D Jr. 2003 *AIAA J.* **41** 1391
[22] Ott J D, Oran E S and Anderson J D Jr. 1999 *NASA CR-1999-209401*
[23] Wu M H and Wang C Y 2011 *Combust. Inst.* **33** 2287
[24] Shu C W and Osher S 1988 *J. Comput. Phys.* **77** 439
[25] Wang C, Shu C W, Han W H and Ning J G 2013 *Combust. Flame* **160** 447
[26] Bychkov V, Golberg S, Liberman M and Eriksson L E 1996 *Phys. Rev. E* **54** 3713
[27] Bychkov V, Petchenko A, Akkerman V and Eriksson L E 2005 *Phys. Rev. E* **72** 046307
[28] Liu Y F, Shen H, Zhang D L and Jiang Z L 2018 *Chin. Phys. B* **27** 084703
[29] Yu H, Qi C and Chen Z 2017 *Proc. Combust. Inst.* **36** 3533
[30] Pan J Y, Hu Z, Wei H Q, Pan M Z and Zhou L 2019 *Combust. Flame* **202** 1
[31] Pan J Y, Wei H Q, Shu G Q, Chen Z and Zhao P 2016 *Combust. Flame* **174** 179